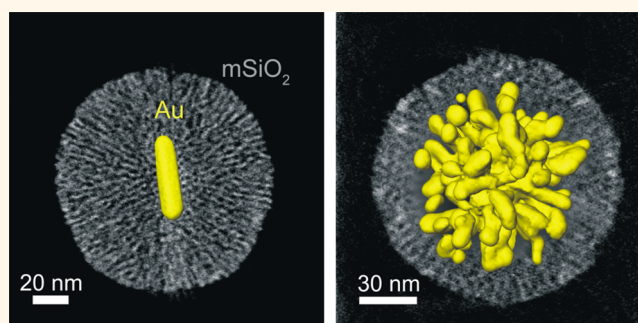


# Templated Growth of Surface Enhanced Raman Scattering-Active Branched Gold Nanoparticles within Radial Mesoporous Silica Shells

Marta N. Sanz-Ortiz,<sup>†</sup> Kadir Sentosun,<sup>‡</sup> Sara Bals,<sup>‡</sup> and Luis M. Liz-Marzán<sup>\*,†,§</sup>

<sup>†</sup>Bionanoplasmonics Laboratory, CIC biomaGUNE, 20009 Donostia-San Sebastián, Spain, <sup>‡</sup>EMAT-University of Antwerp, Groenenborgerlaan 171, B-2020 Antwerp, Belgium, and <sup>§</sup>Ikerbasque, Basque Foundation for Science, 48013 Bilbao, Spain

**ABSTRACT** Noble metal nanoparticles are widely used as probes or substrates for surface enhanced Raman scattering (SERS), due to their characteristic plasmon resonances in the visible and near-IR spectral ranges. Aiming at obtaining a versatile system with high SERS performance, we developed the synthesis of quasi-monodisperse, nonaggregated gold nanoparticles protected by radial mesoporous silica shells. The radial mesoporous channels were used as templates for the growth of gold tips branching out from the cores, thereby improving the plasmonic performance of the particles while favoring the localization of analyte molecules at high electric field regions: close to the tips, inside the pores. The method, which additionally provides control over tip length, was successfully applied to gold nanoparticles with various shapes, leading to materials with highly efficient SERS performance. The obtained nanoparticles are stable in ethanol and water upon thermal consolidation and can be safely stored as a powder.



**KEYWORDS:** plasmonics · SERS · gold nanorods · gold nanostars · mesoporous silica · radial pores

Noble metal nanoparticles are extensively used as substrates for surface-enhanced spectroscopy applications relying on their plasmonic properties.<sup>1–5</sup> Even though the plasmonic behavior is not unique for noble metal nanoparticles, gold, silver, and copper display resonant frequencies at the visible and near-IR regions of the electromagnetic spectrum, rendering them suitable for many practical applications. These nanoparticles act as antennas for light, since under resonance conditions they accommodate oscillating electric fields at their surface with the same frequency as the incident light, but with several orders of magnitude higher intensities. The plasmonic performance can be largely affected by various factors, such as the nanoparticles' composition, their size and shape, the surrounding medium, and their aggregation state. Recent advances in nanoparticle synthesis and characterization have provided

tailored and reproducible preparation methods, so that nanoparticles are widely used for the analysis of the enhanced emitted (surface enhanced fluorescence, SEF) and scattered light (surface enhanced Raman scattering, SERS) by molecules placed in their close surroundings.<sup>6,7</sup> The case of Raman scattering is particularly interesting since it is a highly selective technique (through molecule-specific vibrational fingerprints), which can be applied to a wide range of analytes but has limitations due to the extremely low values of Raman scattering cross sections.<sup>8</sup> SERS relies on the above-mentioned increase in the electric field intensity at the surface of the particles, which results in a large improvement of the detection limit, up to 10 orders of magnitude higher for SERS than for Raman scattering. Therefore, the enhancement of Raman scattering strongly depends on the plasmonic efficiency and thus on the morphology of

\* Address correspondence to  
lizmarzan@cicbiomagune.es.

Received for review July 30, 2015  
and accepted September 15, 2015.

Published online  
10.1021/acsnano.5b04744

© XXXX American Chemical Society

the nanoparticles.<sup>9,10</sup> Additionally, due to the fast decay of the electric field enhancement with the distance from the particle surface, close contact between the analyte and the surface of the nanoparticle is required to obtain an enhanced Raman signal.<sup>6</sup> As a consequence, most studies involve thiolated molecules because they present a high affinity toward gold and silver surfaces.<sup>5,11</sup> For molecules with no special affinity to metals, only randomly adsorbed molecules contribute, whereas the Raman scattering of most of the analyte is negligible. Therefore, sufficient enhancement and suitable detection limits require not only efficient plasmonic response, typically obtained using anisotropic nanostructures containing sharp features or small gaps at which localized regions with higher electric fields are generated (hot spots), but also adsorption of the analyte molecules precisely at such hot spots.<sup>12</sup> Although numerous methods have been developed, it is still difficult to carry out SERS experiments in solution (average SERS) with sufficient sensitivity and generality. Aggregated nanoparticles are often used to improve plasmonic enhancement through hot spot formation, but the aggregation process is often uncontrolled and results in poor reproducibility,<sup>13</sup> so the use of single nanoparticles with optimized morphology is highly preferred.<sup>14,15</sup> On the other hand, improvement of colloidal stability (even for clusters) is typically achieved *via* encapsulation within oxide (silica, titania) or polymer shells.<sup>16,17</sup> By covering each particle with a thick shell (several tenths of a nanometer) it is ensured that no contact exists between metal particles, thereby avoiding uncontrolled hot spot formation. This may have the additional advantage of trapping analyte molecules inside the shell during synthesis, improving control over their location around the particle.<sup>18</sup> The drawback in this case is again that the synthesis must be designed for each specific measurement. A more versatile family of SERS probes can be obtained by using porous coatings,<sup>19</sup> so that the metal particles remain protected from aggregation while their surface is still accessible to the analytes. This approach widens the potential applications of these particles, since the porosity of the shell may lead to size-selective detection of analytes. Importantly, biocompatible mesoporous coatings such as silica have been widely proposed for drug delivery applications.<sup>20,21</sup> With the aim of improving both the enhancement efficiency and the reliability and reproducibility of SERS measurements, we synthesized branched gold nanoparticles coated with mesoporous silica shells containing radially oriented channels, which were used as both templates for seeded growth of branches from the gold cores and traps for analyte adsorption.

## RESULTS AND DISCUSSION

The synthesis of silica-coated branched gold nanoparticles requires a first step in which gold nanoparticles

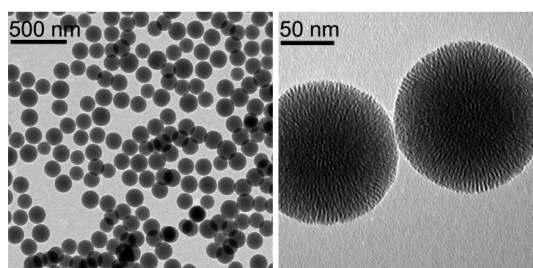


**Figure 1.** Representative TEM images of mesoporous silica nanoparticles with radially oriented channels. Particles show no aggregation and low polydispersity. The pores (ca. 2.1 nm diameter) could be observed at high magnification under slight underfocus.

are coated with mesoporous silica shells with pores extending radially from the center toward the outer particle surface. This is an important advantage over previous reports<sup>22</sup> in which a dense silica shell covered the metal particles, thereby preventing direct contact of the adsorbed molecules with the metallic surface. Additionally, the geometry of the mesoporous channels renders the shell a suitable template for the seeded growth of thin branches from the metal cores, in such a way that analytes entering the channels will accumulate near the tips, where the electric field enhancement is maximum, which is essential for SERS applications.

Mesoporous silica particles are usually obtained through surfactant-templated synthesis adapted from the Stöber method, where the pore radius is determined by the size of templating surfactant micelles. Silica is then formed by hydrolysis of an alkoxy silane (often tetraethoxysilane, TEOS) and condensation in the presence of the self-assembled micelles. Depending on the length of the surfactant chain, different pore sizes are obtained, ranging from 2 nm up to 30 nm.<sup>23</sup> Although cetyltrimethylammonium bromide (CTAB) is probably the most widely used surfactant for mesoporous silica formation, the organization of the pores and the quality of the obtained silicon oxide are easily affected by many interconnected parameters, including the solvent (generally a mixture of ethanol and water), the CTAB/TEOS molar ratio, temperature, stirring speed, pH, or reaction time. Minor changes in the synthesis conditions may yield either disordered pores<sup>24,25</sup> or pores arranged in parallel<sup>23</sup> or radial distribution.<sup>26</sup> Polydispersity and colloidal stability can also be affected by small changes in the reaction parameters, whereas the size of the pores is less sensitive, as it is determined by the micelles.

We developed and optimized a synthesis method that allowed us to obtain nonaggregated, quasi-monodisperse mesoporous silica particles containing mesoporous channels with radial orientation (Figure 1). We used CTAB as templating surfactant, obtaining pores with an average diameter of 2.1 nm, as determined by transmission electron microscopy (TEM).

The synthesis was performed in basic medium, obtained by adjusting the pH with ammonia to a value of around 10. Interestingly, when NaOH was used instead, the obtained particles were highly aggregated, and no conclusion could be made from TEM image analysis regarding the presence of channels or their orientation (Figure S1). No aggregation was observed when the optimized method was used, which involved a low concentration of silica precursors (see discussion below), and using mechanical stirring to obtain particles with a narrow size distribution. This synthesis method was inspired by a recent report describing the preparation of mesoporous silica films on extended surfaces, where mesoporous silica particles were obtained as a byproduct.<sup>27</sup> Even though the experimental conditions differ only slightly, the silica particles obtained in ref 27 display parallel pores, whereas we obtained radial ones, illustrating the high sensitivity of the method to synthesis parameters.

Coating of gold nanoparticles with silica is a popular technique for the development of nanomaterials with plasmonic applications for improved detection,<sup>25</sup> drug delivery,<sup>21</sup> and catalysis.<sup>28,29</sup> The growth of uniform silica shells over gold particles often requires priming of the gold surface to increase its affinity with silica, which can be achieved using silane coupling agents.<sup>30</sup> However, when mesoporous silica is grown on CTAB-stabilized Au nanoparticles (*e.g.*, nanorods), no other functionalization is required and silica shells can be grown in one step using the nanoparticles as nucleation sites,<sup>25</sup> since the capping surfactant (CTAB) is also used as a template for the formation of the porous shells. Although the obtained pores are usually disordered, a recent report showed the formation of mesoporous silica with radial pores on gold nanoparticles,<sup>22</sup> which however involved the deposition of a dense silica layer on the particles prior to growing the mesoporous shell, somehow limiting the potential applications of the material. We report here the synthesis of radially oriented mesoporous silica-coated gold nanoparticles with no need for a buffer layer of dense silica.

We used gold particles with different morphologies as nucleation sites: spheres, single-crystal nanorods, pentatwinned nanorods, and nanotriangles, all of them capped with CTAB, even if initially synthesized with different capping molecules. Representative TEM images of the different nanoparticles after growth of mesoporous silica shells with radial pores are displayed in Figures 2 and S2. Detailed analysis of the TEM images confirmed that every individual gold particle was uniformly covered by silica, and just a few core-free silica particles were formed as byproduct (Figure S2). The extinction spectra of these particles are also provided as Supporting Information (Figure S3). We obtained in all cases nonaggregated particles with homogeneous silica coverage and shell thickness.

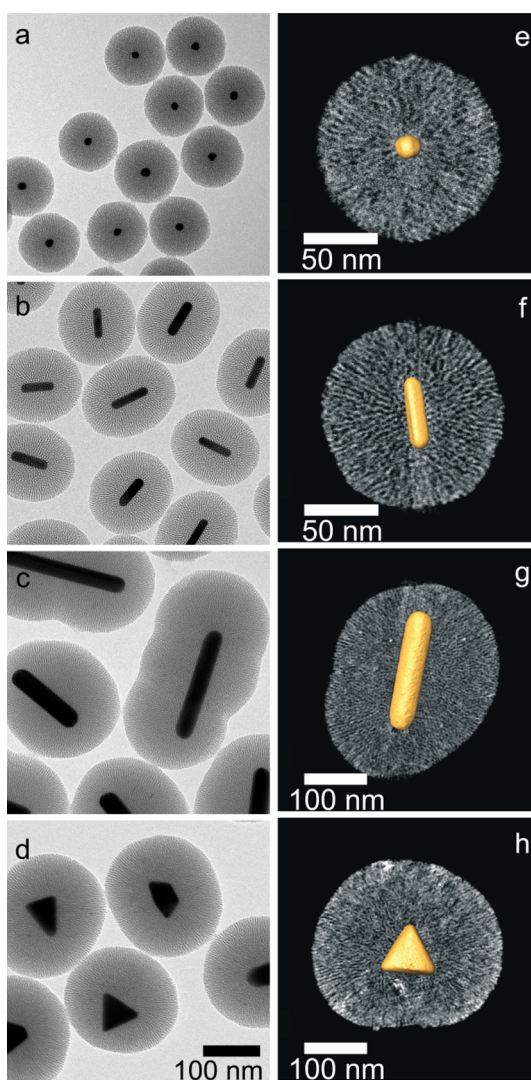


**Figure 2.** 2D and 3D TEM characterization of hybrid nanostructures containing gold nanoparticles with various shapes: nanospheres (a, e), single-crystal nanorods (b, f), pentatwinned nanorods (c, g), and nanotriangles (d, h). The radial mesopores in the silica shells can be observed in the visualizations of the 3D reconstructions in the right panel (the Au nanoparticle and the silica shell are displayed in yellow and white, respectively). All the images in the left panel were obtained at the same magnification.

Unfortunately, coating of gold nanostars resulted in reshaping into quasi-spherical particles, which was likely due to the effect of the temperature (60 °C) required for the formation of the silica shell.<sup>31,32</sup> TEM was also used (under slight underfocus) to verify the presence and arrangement of the pores, which were indeed found to grow radially, fully connecting the gold–silica interface to the outer surface of the particles. Further characterization of the three-dimensional morphology of silica-coated gold particles was performed using electron tomography; that is, 2D projection images at different angles were collected by ADF and HAADF detectors simultaneously in scanning transmission electron microscopy (STEM) mode, which enabled us to characterize the beam-sensitive silica

shells in a dose-efficient way (for more information see ref 33). Visualizations of the resulting 3D reconstructions are presented in Figure 2 and Supporting Video S1, clearly revealing the radial orientation of the pores in the silica shells in all cases. The pore size and the interpore wall thickness of the SiO<sub>2</sub> shells were determined by analyzing orthoslices through the 3D reconstructions. In total, 200 measurements based on four different reconstructions were performed to obtain statistically relevant results, yielding an average pore size of  $2.10 \pm 0.3$  nm and average silica wall thickness of  $2.40 \pm 0.4$  nm (the corresponding histograms are shown in Figure S4). In addition, energy-dispersive X-ray (EDX) analysis revealed a perfect separation between the Au core and the silica shell (Figure S5).

It is worth noting that the silica shell growth is rather slow, which allowed us to carry out a time-resolved study of the morphological evolution. Although after the first 3 h all gold particles were already fully covered, the final thickness was reached only after 24 h (Figure S6). Formation of the pore structure was observed to be a dynamic process, the final structure being well defined after an additional period of 24 h. The slow organization of the pores into the regular radial arrangement was favored by a relatively high reaction temperature (60 °C). In fact, the particles could be recovered by centrifugation after 24 h, redispersed in ethanol, and stored at 60 °C for another 24 h period, yielding an identical result and stability. Interestingly, the shell morphology partially followed the shape of the gold cores, being isotropic for spheres, whereas for both types of nanorods and for nanotriangles the outer curvature of the silica shell changed according to that of the core (Figures 2 and S2). In particular, the longer pentatwinned nanorods present a complex coating resembling several silica spheres linked to each other, which is likely to arise from a nonuniform silica growth process, *i.e.*, not starting simultaneously all over the surface. The thickness of the silica shells could be tailored by simply varying the amount of gold particles introduced as seeds (Figure S7). Improved control over the shell thickness can be obtained through modulation of other synthesis parameters, such as pH and stirring rate.

An important feature toward potential applications is the stability of the particles in various solvents. All the synthesized particles were stable in ethanol for over one year, but could also be dried up for storage as a powder (Figure S7) and then dispersed in ethanol by sonication for a few minutes. However, stability in water is limited to a few hours (Figure S8) due to partial dissolution of the silica shell, which strongly affects the structure of the mesopores. This is a common finding in many colloidal silica and silica-coated nanoparticles.<sup>34</sup> Notwithstanding, the resilience of silica can be improved by subjecting the particles to a high-temperature

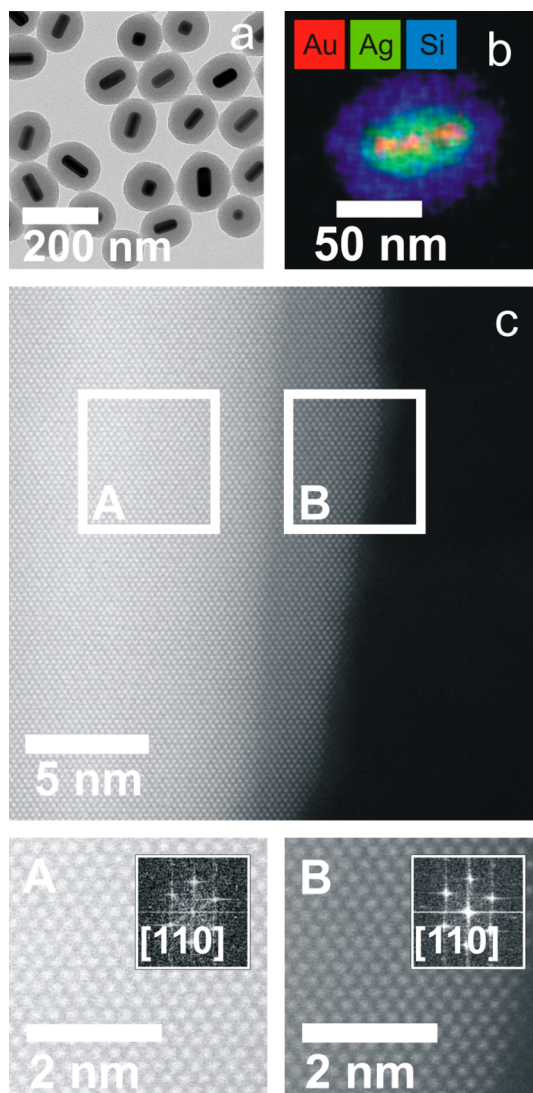


**Figure 3.** Single-crystal gold nanorods covered with a mesoporous silica layer with radial pores, after *in situ* growth of a silver layer through the silica pores. (a) Low-magnification TEM image; (b) EDX map; (c) HAADF-STEM image showing uneven Ag shell thickness and epitaxial growth of the silver layer on the gold core. The crystallinity and the epitaxial relation of the gold core and the silver shell can be observed in the high-resolution images and corresponding fast Fourier transforms (acquired from the areas labeled as A and B in panel c).

treatment (up to 550 °C) of the dry powder, which not only consolidates the silica shells but also removes remaining traces of CTAB from the pores through calcination of organic matter.<sup>35</sup> For the mesoporous silica-coated particles, a compromise between improving stability in water while avoiding thermal reshaping of the gold cores was achieved by treating the particles at an intermediate temperature of 300 °C. When such a milder thermal treatment was applied to anisotropic silica-coated gold particles, their chemical stability in water was improved over one month, and only a slight reshaping and decrease of anisotropy was observed to occur, leading to changes of their aspect ratio and in

turn of their respective plasmon resonance frequencies (Figure S9). Temperature treatment can in fact be used as an additional handle to tune the plasmonic response of the coated particles, but milder temperature treatments (up to 100 °C) can also be applied to enhance silica shell stability on both nanorods and nanotriangles, causing a minimum reshaping but improving stability in water up to a few days (Figure S8). Importantly, prior to the thermal treatment CTAB should be removed from the pores by washing with 1 M HCl in ethanol.

A clear advantage of the accessibility of the gold nanoparticles through the radial pores is that gold-catalyzed chemical reactions can take place selectively at the cores. An obvious example is the growth of a silver layer over the gold cores, which would additionally provide a superior plasmonic performance. Silver coating was carried out by *in situ* reduction of  $\text{Ag}^+$  ions by ascorbic acid, resulting in complete coating of the central Au cores (nanorods in this case), as shown in Figure 3. High-resolution electron microscopy analysis showed that silver grows epitaxially over the gold cores and the silver shell thickness could be modified by simply changing the (seed) particle concentration in the silver growth solution. It is important to note that this experiment was carried out using silica-coated nanorods without thermal treatment, thus resulting in partial damage of the mesoporous silica structure, which is likely responsible for the uniform silver coating. The corresponding optical changes are shown in Figure S10 and are in agreement with previous observations using noncoated nanorods.<sup>36</sup>

We next aimed at growing Au tips from the central cores, using the radial mesopores as templates, which were expected to enhance SERS performance through formation of regions with high electric field enhancement at sharp features, while localizing analyte molecules at such hot spots. The use of mesoporous silica as a template to grow metal branches from nanoparticles has been previously demonstrated for gold particles embedded in mesoporous silica films.<sup>37</sup> We carried out an overgrowth reaction based on a modification of a synthesis method for gold nanostars, which involves the reduction of  $\text{HAuCl}_4$  in the presence of silver ions.<sup>38</sup> By using the silica-coated particles as seeds, the radial silica channels could act as templates, so that thin and short gold wires would branch out from the surface of the gold cores, regardless of the initial core shape, as observed by TEM (Figures 4 and S11). Importantly, the pores remained stable after gold branching. The way the gold branches grow their way out of the cores through the silica channels can be clearly appreciated from 3D visualizations of different structures after tip growth (Figure 4, Supporting Videos S2 and S3). The tip width of the branches could be extracted from the 3D reconstructions and was estimated to be 3.5 nm ( $\pm 1$  nm), *i.e.*, slightly larger than the pore size, probably

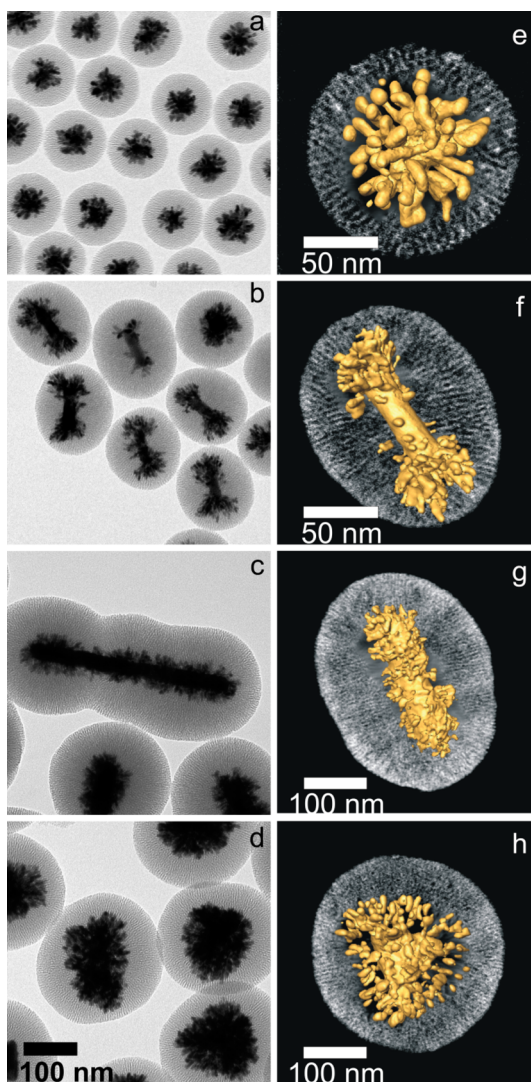


**Figure 4.** 2D and 3D TEM characterization of hybrid nanostructures containing different gold nanoparticles coated with mesoporous silica, after growing gold tips through the silica channels: nanospheres (a, e), single-crystal nanorods (b, f), pentatwinned nanorods (c, g), and nanotriangles (d, h). All the images in the left panel were obtained at the same magnification. In the right panel, a visualization of the 3D reconstructions for a representative nanoparticle of each type is displayed, where the radial nature of both the channels and the gold branches can be observed.

because the gold branches push their way through the channels during growth. High-resolution TEM images of spheres with tips show that both the gold core before the branching process and the branches themselves are polycrystalline (Figures 5 and S12).

An important aspect of this synthesis, in particular for plasmonic applications, is the colloidal stability of the particles (no aggregation) and the absence of homogeneous nucleation of gold particles in solution (see low-magnification TEM images in Figure S11). We can thus state that gold reduction is catalyzed by the gold cores, and thus gold branches grow preferentially over them, in a fast reaction that is completed within a few seconds. Although most of the particles

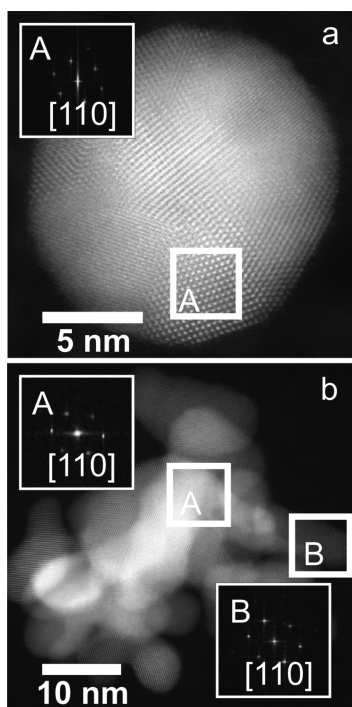


**Figure 5.** High-resolution electron micrographs and respective fast Fourier transform patterns of spherical cores before (a) and after (b) tip growth, in both cases demonstrating polycrystallinity.

have similar tip lengths, few of them were found to contain either no tips or particularly long ones, which is likely related to the fast reaction rate. Aggregation was observed only when the concentration of seed particles was too low, since in those cases the tips can actually reach the silica shell surface and bridge to neighboring particles. Although branching was achieved on various types of nanoparticle cores, a significant difference was noticed between single-crystal nanorods and other morphologies. In the case of spheres, pentatwinned nanorods, and nanotriangles, branching occurred uniformly from spots on the entire particle surface (Figures 4 and S11). Instead, branching from single-crystal nanorods was mainly observed to occur at their ends, which was confirmed by electron tomography reconstruction (Figure 4f and Supporting Video S3). This anomaly is however in accordance with a recent report by our group, regarding the growth of tips from bare (noncoated) single-crystal gold nanorods<sup>39</sup> and is likely related to the presence of silver or silver bromide, preferentially on the lateral facets of the nanorods, although the precise role and localization of silver or silver halides in anisotropic gold nanoparticles is not yet sufficiently understood.<sup>40,41</sup> From the optical point of view, the growth of tips on gold nanoparticles has been reported to result in the red shift and broadening of the corresponding localized surface plasmon resonance band.<sup>38,39</sup> This effect was indeed observed here, as exemplarily shown for spheres in Figure 6. This effect

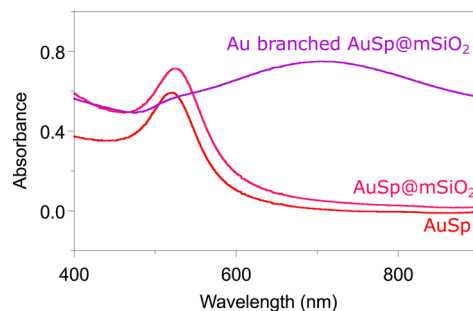


**Figure 6.** Evolution of the extinction spectra for the same particle concentration of 15 nm gold spheres stabilized in 0.1 M CTAB, after mesoporous silica shell growth, and after templated tip growth.

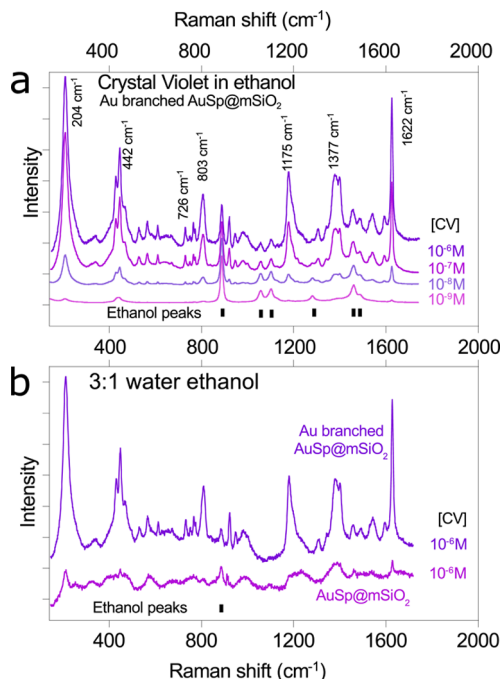


**Figure 7.** (a) SERS spectra of CV in ethanol at selected concentrations. (b) SERS spectra recorded from a  $10^{-6}$  M CV solution in a water/ethanol (3:1) mixture, using Au spheres coated with mesoporous silica before ( $\text{AuSp@mSiO}_2$ ) and after ( $\text{Au-branched AuSp@mSiO}_2$ ) templated branching. All spectra were obtained using colloids with the same concentration as  $\text{Au}^0$  (0.25 mM), upon laser excitation at 633 nm. Vertical offset was applied for clarity.

has important consequences regarding potential applications of these nanoparticles in biological systems, as electromagnetic field enhancement can be achieved by irradiation in the near-IR, *i.e.*, in the biological transparency window.

We finally tested the SERS performance of branched mesoporous silica-coated gold spheres in solution. Colloidal dispersions containing a fixed gold concentration ( $[\text{Au}^0] = 0.25$  mM) were employed for SERS detection of two model analytes, which were specifically chosen not to chemically bind to gold: Crystal Violet (CV) and Nile Blue (NB). Representative results are displayed in Figures 7 and S13, respectively, showing detection of concentrations as low as  $10^{-9}$  M for

CV and  $10^{-8}$  M for NB. Several characteristic peaks of both analytes are indicated in the spectra:  $204\text{ cm}^{-1}$  (benzene breathing mode),  $442\text{ cm}^{-1}$  (16a),  $726\text{ cm}^{-1}$  (4),  $803\text{ cm}^{-1}$  (10a),  $1175\text{ cm}^{-1}$  (9a),  $1377\text{ cm}^{-1}$  (e), and  $1622\text{ cm}^{-1}$  (8a) among others for CV<sup>42</sup> and  $1647\text{ cm}^{-1}$  ( $\text{NH}_2$  deformation) and  $593\text{ cm}^{-1}$  (benzene breathing mode) for NB.<sup>43</sup> The spectra also contain Raman scattering peaks corresponding to ethanol, which was used as a solvent (Figures 7a and S13). Since the intensity of the ethanol peaks does not depend on analyte concentration, they were used to normalize the intensity of the different SERS spectra, so as to compensate for possible variations of laser power and focus. Thermally treated particles also displayed efficient performance, as demonstrated in Figure 7b. For these spectra, ethanol in a 1:3 ratio was added to the aqueous solution, again for normalization of the SERS signal. The superior performance of branched nanoparticles for SERS detection in water is demonstrated in Figure 7b, where SERS spectra of CV ( $10^{-6}$  M) in the presence of nanospheres with and without tips are compared, using in both cases a  $\text{Au}^0$  concentration of 0.25 mM. Even though (for the same concentration of metal) the number of branched nanoparticles per unit volume was estimated to be *ca.* 6-fold smaller than that of spherical particles, the signal obtained from the former was 1 order of magnitude more intense than that from the latter. We note additionally that the limit of detection for CV was  $10^{-6}$  M using spherical nanoparticles under the selected experimental conditions, whereas for branched nanoparticles it was possible to detect CV concentrations up to 4 orders magnitude lower (Figure 7a). These results are in agreement with reported electromagnetic simulations

for spheres and nanostars, which predict that the near-field enhancement for single nanostars can be on the order of  $10^4$ ,<sup>44</sup> whereas typical values for spheres are *ca.* 2 orders of magnitude lower.<sup>45</sup> Interestingly, from the analysis of the dependence of the normalized intensity of several CV peaks with dye concentration (Figure S14) it can be concluded that the amount of dye molecules per particle approached saturation. We thus expect that the detection limit can be further improved *via* selection of the most suitable nanoparticle morphology and optimization of the concentration of nanoparticles and the amount of analyte molecules per particle.

## CONCLUSIONS

We developed a synthetic method for the preparation of gold nanoparticles coated with mesoporous silica shells displaying radial orientation of pores. The mesopores in the silica shells were used as templates for the seeded growth of gold tips branching from the surface of the gold cores. The method was successfully implemented for gold nanoparticles with various morphologies, thereby showing a wide versatility and general application. The resulting hybrid particles are stable for extended periods of time if stored in ethanol or as a powder, but can also be stored in water after a suitable thermal treatment. The radial structure of the pores and the growth of the tips through them favor the localization of analyte molecules in close proximity to hot spots, as indicated by SERS measurements. All these features render these particles a particularly versatile family of SERS probes: easily tunable, stable in various media, and suitable for biological applications.

## MATERIALS AND METHODS

**Chemicals.** Tetrachloroauric acid trihydrate ( $\text{HAuCl}_4 \cdot 3\text{H}_2\text{O}$ ,  $\geq 99.9\%$ ), cetyltrimethylammonium bromide (CTAB), benzyltrimethylammonium chloride (BDAC), L-ascorbic acid ( $\geq 99.9\%$ ), silver nitrate ( $\text{AgNO}_3$ , 99%), tetraethoxysilane (TEOS, 98%), sodium borohydride ( $\text{NaBH}_4$ , 99%), Crystal Violet, and Nile Blue were purchased from Sigma-Aldrich and used as received. Synthesis grade ethanol ( $>99.9\%$ , absolute grade), ammonia and hydrochloric acid were also purchased from Sigma-Aldrich. Water was purified by a Milli-Q system (resistivity  $18.2\text{ M}\Omega \cdot \text{cm}$  at  $25\text{ }^\circ\text{C}$ ). All glassware was washed with hydrofluoric acid (5 vol % in water), rinsed with water, and washed with *aqua regia*, then rinsed with tap water, washed 3-fold with Milli-Q water, and dried before use.

**Gold Nanoparticles.** Gold spheres were synthesized by the sodium citrate reduction method,<sup>46</sup> and single-crystal gold nanorods were prepared as described in ref 47, whereas nanostars were obtained by a surfactant-free method using 15 nm citrate gold spheres as seeds.<sup>38</sup> Pentatwinned nanorods and nanotriangles were synthesized according to previously reported methods.<sup>48,15</sup> The concentration of  $\text{Au}^0$  in all gold colloids was derived from their extinction spectra (absorbance at  $400\text{ nm}$ ).<sup>47,49</sup>

**Mesoporous Silica Particles with Radial Pores.** This synthesis has been proven to work for reaction volumes between 10 and 500 mL. As an example, for a final synthesis volume of *ca.* 250 mL we prepared 175 mL of a 6 mM aqueous CTAB solution in a 500 mL round beaker. All reactants were added while stirring and maintaining the solution temperature between

30 and  $35\text{ }^\circ\text{C}$ . The beaker should be kept closed throughout the reaction to avoid solvent evaporation. When 75 mL of ethanol was poured in the CTAB solution, the solution turned slightly cloudy but became transparent again upon stirring. At this point  $100\text{ }\mu\text{L}$  of  $\text{NH}_3$  (25 vol %) was added to achieve a pH value close to 10. Finally  $200\text{ }\mu\text{L}$  of TEOS was added dropwise under vigorous stirring, and the solution was then heated to  $60\text{ }^\circ\text{C}$  and maintained at this temperature for 3 days under gentle stirring. Although a magnetic stirrer can be used, a mechanical stirrer is preferred, as it was found to produce particles with a narrower size distribution. The solution turned white after a few hours due to formation of a high concentration of silica particles that significantly scatter light. After 3 days, the particles are recovered by centrifugation (60 min; 7500–9000 rpm;  $35\text{ }^\circ\text{C}$ ). The centrifugation time and speed can be increased if required to recover all the particles, which could then be dispersed in ethanol and washed by centrifugation and redispersion.

**Mesoporous Silica-Coated Gold Particles.** The procedure is the same as that for the synthesis of mesoporous silica particles but using presynthesized Au particles as nucleation sites for silica shell growth. Gold nanoparticles were first dispersed in 0.1 M CTAB and then concentrated by centrifugation and redispersion in *ca.* 2% of the final synthesis volume (*e.g.*, 5 mL for a total synthesis volume of 250 mL). This synthesis was tested for volumes ranging from 10 to 500 mL. For a 250 mL final volume, 170 mL of a 6 mM CTAB solution was mixed with 75 mL of ethanol at a temperature between 30 and  $35\text{ }^\circ\text{C}$  in a 500 mL

round beaker under mechanical stirring. Once the temperature was stabilized and the solution was transparent and free of bubbles, 100  $\mu\text{L}$  of  $\text{NH}_3$  (25 vol %) was added. Subsequently, 5 mL of the gold particle solution was poured into the synthesis solution. After 5 min to ensure homogeneity of the solution, 200  $\mu\text{L}$  of TEOS was added dropwise under vigorous stirring. The temperature was then set to 60  $^\circ\text{C}$  for the remaining reaction time. A slight increase in turbidity of the colloid due to silica shell formation was observed after 2–3 h. After 2 days, the particles were recovered by centrifugation (30 min; 7500–9000 rpm; 35  $^\circ\text{C}$ ) and washed twice in ethanol. The optimum concentration of the gold seed solution was determined to be 5 mM (0.1 mM in the total reaction volume), but it could be varied from 2 mM to 10 mM to adjust the silica shell thicknesses. Higher gold nanoparticle concentrations may lead to aggregation before the silica shell has been formed. On the other hand, when the TEOS concentration was below the optimal range, each hybrid nanoparticle was found to contain multiple gold cores, whereas high TEOS concentrations led to nucleation of bare mesoporous silica particles. The resulting particles are stable in ethanol and can be dried and stored as a powder and subsequently redispersed in ethanol by sonication.

**CTAB Removal from the Silica Pores.** For mesoporous silica particles the CTAB template is usually removed by calcination. A thermal treatment at 550  $^\circ\text{C}$  for 4 h was successfully used for pure silica particles but could not be applied to silica-coated gold particles, as it results in reshaping of the gold cores. Most CTAB molecules can however be removed by thorough washing with ethanol, as the solubility of CTAB is higher in ethanol than in water. This method can be further improved by washing in ethanol under reflux for 4 h. Alternatively, a faster cleaning procedure would comprise an extra washing step with HCl (1 M in ethanol) after the first wash in ethanol, but the particles should then be washed twice again by centrifugation in ethanol to remove excess HCl. Calcination is still useful to improve the stability of the silica shell in water and avoid dissolution. Different temperature treatments were applied to the mesoporous silica-coated gold particles, observing that higher temperatures lead to more stable particles. When treated at 550  $^\circ\text{C}$ , anisotropic nanoparticles were invariably found to reshape into more isotropic shapes, so milder temperature treatments were preferred. In a first step, the samples were dried in an oven at 60  $^\circ\text{C}$ ; then the temperature was increased to 100  $^\circ\text{C}$  and maintained for 1 h, thereby improving the stability of the shell for a few days while preserving the shape and optical response of the particles. In a second step, the samples were treated at 300  $^\circ\text{C}$  for 2 h, leading to much higher stability (over one month in water) but with a slight reshaping of the gold cores and their plasmonic properties. Upon cooling to room temperature, the particles can be stored as a powder or redispersed in water or ethanol.

**Au Branching through Silica Pores.** The growth of gold branches through the pores of silica-coated particles was carried out using a method previously developed to grow surfactant-free nanostars,<sup>37</sup> using the mesoporous silica-coated gold particles as seeds. In brief, 50  $\mu\text{L}$  of HCl 1 M was added to 50 mL of 0.25 mM  $\text{HAuCl}_4$  solution and stirred for 5 min, and then 2.5 mL of the seed solution in water was added under vigorous stirring, followed by 500  $\mu\text{L}$  of 3 mM  $\text{AgNO}_3$  and 250  $\mu\text{L}$  of 0.1 M ascorbic acid in this order, leading to a sudden color change to blue. After 10 min the particles were recovered by centrifugation (30 min; 7500–9000 rpm; 35  $^\circ\text{C}$ ) and washed twice with ethanol. The standard gold concentration in the seed solution was 1 mM, but it could be varied to modify the length of the tips. Concentrations between 0.5 and 4 mM were proven to work without particle aggregation.

**Ag Growth on Au Cores.** Mesoporous silica-coated gold particles were transferred into a 10 mM BDAC solution in water under mild stirring. Separately, 100  $\mu\text{L}$  of 0.1 M  $\text{AgNO}_3$  was mixed with 10 mL of an aqueous 10 mM BDAC solution and 400  $\mu\text{L}$  of 0.1 M ascorbic acid, and then 1 mL of the seed solution in BDAC ([Au] = 5 mM) was added. Protection against light and a temperature of 65  $^\circ\text{C}$  are recommended. After 3 h the heating was turned off, and after cooling to room temperature the particles were recovered and washed by centrifugation and redispersion in ethanol. This synthesis was adapted from ref 50.

**Characterization.** Optical extinction spectra were recorded using an Agilent 8453 UV–vis–NIR photodiode array spectrophotometer. SERS spectra were recorded using a Renishaw InVia Raman microscope equipped with two Peltier-cooled CCD detectors and a Leica microscope with two gratings with 1200 and 1800 lines/mm and band-pass filter optics. Transmission electron microscopy images were collected using a JEOL JEM-1400PLUS instrument operating at 120 kV. Samples for electron tomography were prepared by casting drops on a Quantifoil carbon TEM grid. Tilt angle series were acquired using a FEI Tecnai Osiris electron microscope, operated at 120 kV, and a dedicated tomography holder (Fischione Instruments, model 2020). Scanning transmission electron microscopy with high angle annular dark-field detection (HAADF-STEM) and ADF-STEM series were collected simultaneously using two different annular dark-field detectors at tilt angles in the range  $\pm 72^\circ$ , with 3 $^\circ$  increments. A detailed description of the tomography reconstruction procedure is provided in ref 33.

**Conflict of Interest:** The authors declare no competing financial interest.

**Acknowledgment.** This work has been funded by the European Research Council (ERC Advanced Grant 267867 Plasmaquo and Starting Grant Colouratom). The research leading to these results has received funding from the European Union's Seventh Framework Programme (FP7/2007–2013 under grant agreement no. 312184, SACS). Help from Mert Kurttepelii is acknowledged. Pentatwinned nanorods and nanotriangles were synthesized by L. Scarabelli.

**Supporting Information Available:** The Supporting Information is available free of charge on the ACS Publications website at DOI: 10.1021/acs.nano.5b04744.

Additional TEM images, extinction spectra, and EDX analysis (PDF)  
3D tomography reconstruction of a silica coated Au nanorod (MPG)  
3D visualizations of an Au nanosphere after tip growth (MPG)  
3D visualizations of a single crystal Au nanorod after tip growth (MPG)

## REFERENCES AND NOTES

- Fong, K. E.; Yung, L.-Y. L. Localized Surface Plasmon Resonance: A Unique Property of Plasmonic Nanoparticles for Nucleic Acid Detection. *Nanoscale* **2013**, *5*, 12043–12071.
- Mayer, K. M.; Hafner, J. H. Localized Surface Plasmon Resonance Sensors. *Chem. Rev.* **2011**, *111*, 3828–3857.
- Garcia, M. A. Surface Plasmons in Metallic Nanoparticles: Fundamentals and Applications. *J. Phys. D: Appl. Phys.* **2012**, *45*, 389501.
- Schlücker, S. Surface-Enhanced Raman Spectroscopy: Concepts and Chemical Applications. *Angew. Chem., Int. Ed.* **2014**, *53*, 4756–4795.
- Alvarez-Puebla, R.; Liz-Marzan, L. M.; Garcia de Abajo, F. J. Light Concentration at the Nanometer Scale. *J. Phys. Chem. Lett.* **2010**, *1*, 2428–2434.
- Alvarez-Puebla, R. A.; Liz-Marzán, L. M. SERS Detection of Small Inorganic Molecules and Ions. *Angew. Chem., Int. Ed.* **2012**, *51*, 11214–11223.
- Fort, E.; Grésillon, S. Surface Enhanced Fluorescence. *J. Phys. D: Appl. Phys.* **2008**, *41*, 013001.
- Patnaik, P. Infrared and Raman Spectroscopy. In *Dean's Analytical Chemistry Handbook*; McGraw-Hill Professional, 2004.
- Moskovits, M. Persistent Misconceptions Regarding SERS. *Phys. Chem. Chem. Phys.* **2013**, *15*, 5301–5311.
- LeRu, E. C.; Meyer, M.; Etchegoin, P. G. Surface Enhanced Raman Scattering Enhancement Factors: A Comprehensive Study. *J. Phys. Chem. C* **2007**, *111*, 13794–13803.
- Moores, A.; Goettmann, F. The Plasmon Band in Noble Metal Nanoparticles: An Introduction to Theory and Applications. *New J. Chem.* **2006**, *30*, 1121.
- Alvarez-Puebla, R. A.; Liz-Marzan, L. M. Traps and Cages for Universal SERS Detection. *Chem. Soc. Rev.* **2012**, *41*, 43–51.

13. Polavarapu, L.; Pérez-Juste, J.; Xu, Q.-H.; Liz-Marzán, L. M. Optical Sensing of Biological, Chemical and Ionic Species through Aggregation of Plasmonic Nanoparticles. *J. Mater. Chem. C* **2014**, *2*, 7460–7476.
14. Hrelescu, C.; Sau, T. K.; Rogach, A. L.; Jäckel, F.; Feldmann, J. Single Gold Nanostars Enhance Raman Scattering. *Appl. Phys. Lett.* **2009**, *94*, 2007–2010.
15. Scarabelli, L.; Coronado-Puchau, M.; Giner-Casares, J. J.; Langer, J.; Liz-Marzán, L. M. Monodisperse Gold Nanotriangles: Size Control, Large-Scale Self-Assembly, and Performance in Surface-Enhanced Raman Scattering. *ACS Nano* **2014**, *8*, 5833–5842.
16. Li, W.; Camargo, P. H. C.; Lu, X.; Xia, Y. Dimers of Silver Nanospheres: Facile Synthesis and Their Use as Hot Spots for Surface-Enhanced Raman Scattering. *Nano Lett.* **2009**, *9*, 485–490.
17. Wustholz, K. L.; Henry, A. I.; McMahon, J. M.; Freeman, R. G.; Valley, N.; Piotti, M. E.; Natan, M. J.; Schatz, G. C.; Van Duyne, R. P. Structure-Activity Relationships in Gold Nanoparticle Dimers and Trimers for Surface-Enhanced Raman Spectroscopy. *J. Am. Chem. Soc.* **2010**, *132*, 10903–10910.
18. Fernández-López, C.; Mateo-Mateo, C.; Alvarez-Puebla, R. A.; Pérez-Juste, J.; Pastoriza-Santos, I.; Liz-Marzán, L. M. Highly Controlled Silica Coating of PEG-Capped Metal Nanoparticles and Preparation of SERS-Encoded Particles. *Langmuir* **2009**, *25*, 13894–13899.
19. Liu, W.; Zhu, Z.; Deng, K.; Li, Z.; Zhou, Y.; Qiu, H.; Gao, Y.; Che, S.; Tang, Z. Gold Nanorod@Chiral Mesoporous Silica Core-Shell Nanoparticles with Unique Optical Properties. *J. Am. Chem. Soc.* **2013**, *135*, 9659–9664.
20. Zhang, Z.; Wang, L.; Wang, J.; Jiang, X.; Li, X.; Hu, Z.; Ji, Y.; Wu, X.; Chen, C. Mesoporous Silica Coated Gold Nanorods as a Light Mediated Multifunctional Theranostic Platform for Cancer Treatment. *Adv. Mater.* **2012**, *24*, 1418–1423.
21. Liu, J.; Detrembleur, C.; De Pauw-Gillet, M.-C.; Mornet, S.; Jérôme, C.; Duguet, E. Gold Nanorods Coated with Mesoporous Silica Shell as Drug Delivery System for Remote Near Infrared Light-Activated Release and Potential Phototherapy. *Small* **2015**, *11*, 2323–2332.
22. Yang, J.; Shen, D.; Zhou, L.; Li, W.; Li, X.; Yao, C.; Wang, R.; El-Toni, A. M.; Zhang, F.; Zhao, D. Spatially Confined Fabrication of Core-Shell Gold nanocages@Mesoporous Silica for near-Infrared Controlled Photothermal Drug Release. *Chem. Mater.* **2013**, *25*, 3030–3037.
23. Zhao, D.; Feng, J.; Huo, Q.; Melosh, N.; Fredrickson, G. H.; Chmelka, B. F.; Stucky, G. D. Triblock Copolymer Syntheses of Mesoporous Silica with Periodic 50 to 300 Angstrom Pores. *Science* **1998**, *279*, 548–552.
24. Gorelikov, I.; Matsuura, N. Single-Step Coating of Mesoporous Silica on Cetyltrimethyl Ammonium Bromide-Capped Nanoparticles. *Nano Lett.* **2008**, *8*, 369–373.
25. Abadeer, N. S.; Brennan, M. R.; Wilson, W. L.; Catherine, J.; Murphy, C. J. Distance and Plasmon Wavelength Dependent Fluorescence of Molecules Bound to Silica-Coated Gold Nanorods. *ACS Nano* **2014**, *8*, 8392–8406.
26. Li, Z.; Zeng, H. C. Armored MOFs: Enforcing Soft Microporous MOF Nanocrystals with Hard Mesoporous Silica. *J. Am. Chem. Soc.* **2014**, *136*, 5631–5639.
27. Teng, Z.; Zheng, G.; Dou, Y.; Li, W.; Mou, C. Y.; Zhang, X.; Asiri, A. M.; Zhao, D. Highly Ordered Mesoporous Silica Films with Perpendicular Mesochannels by a Simple Stöber-Solution Growth Approach. *Angew. Chem., Int. Ed.* **2012**, *51*, 2173–2177.
28. Wu, C.; Lim, Z.; Zhou, C.; Guo Wang, W.; Zhou, S.; Yin, H.; Zhu, Y. A Soft-Templated Method to Synthesize Sintering-Resistant Au-Mesoporous-Silica Core-Shell Nanocatalysts with Sub-5 nm Single-Cores. *Chem. Commun.* **2013**, *49*, 3215–3217.
29. Joo, S. H.; Park, J. Y.; Tsung, C.-K.; Yamada, Y.; Yang, P.; Somorjai, G. A. *Nat. Mater.* **2009**, *8*, 126–131.
30. Liz-Marzán, L. M.; Giersig, M.; Mulvaney, P. Synthesis of Nanosized Gold-Silica Core-Shell Particles. *Langmuir* **1996**, *12*, 4329–4335.
31. Barbosa, S.; Agrawal, A.; Rodríguez-Lorenzo, L.; Pastoriza-Santos, I.; Alvarez-Puebla, R. A.; Kornowski, A.; Weller, H.; Liz-Marzán, L. M. Tuning Size and Sensing Properties in Colloidal Gold Nanostars. *Langmuir* **2010**, *26*, 14943–14950.
32. Petrova, H.; Perez Juste, J.; Pastoriza-Santos, I.; Hartland, G. V.; Liz-Marzán, L. M.; Mulvaney, P. On the Temperature Stability of Gold Nanorods: Comparison between Thermal and Ultrafast Laser-Induced Heating. *Phys. Chem. Chem. Phys.* **2006**, *8*, 814–821.
33. Sentosun, K.; Sanz-Ortiz, M. N.; Batenburg, K. J.; Liz-Marzán, L. M.; Bals, S. Combination of HAADF-STEM and ADF-STEM Tomography for Core-Shell Hybrid Materials. *Part. Part. Syst. Charact.* in press.
34. López-Puente, V.; Abalde-Cela, S.; Angelomé, P. C.; Álvarez-Puebla, R. A.; Liz-Marzán, L. M. Plasmonic Mesoporous Composites as Molecular Sieves for SERS detection. *J. Phys. Chem. Lett.* **2013**, *4*, 2715–2720.
35. Kleitz, F.; Schmidt, W.; Schüth, F. Calcination Behavior of Different Surfactant-Templated Mesoporous Silica Materials. *Microporous Mesoporous Mater.* **2003**, *65*, 1–29.
36. Liu, M.; Guyot-Sionnest, P. Synthesis and Optical Characterization of Au/Ag Core/Shell Nanorods. *J. Phys. Chem. B* **2004**, *108*, 5882–5888.
37. Angelomé, P. C.; Pastoriza-Santos, I.; Pérez-Juste, J.; Rodríguez-González, B.; Zelcer, A.; Soler-Illia, G. J. A. A.; Liz-Marzán, L. M. Growth and Branching of Gold Nanoparticles through Mesoporous Silica Thin Films. *Nanoscale* **2012**, *4*, 931–939.
38. Yuan, H.; Khoury, C. G.; Hwang, H.; Wilson, C. M.; Grant, G. a; Vo-Dinh, T. Gold Nanostars: Surfactant-Free Synthesis, 3D Modelling, and Two-Photon Photoluminescence Imaging. *Nanotechnology* **2012**, *23*, 075102.
39. Novikov, S. M.; Sánchez-Iglesias, A.; Schmidt, M. K.; Chuvilin, A.; Aizpurua, J.; Grzelczak, M.; Liz-Marzán, L. M. Gold Spike Nanodumbbells: Anisotropy in Gold Nanostars. *Part. Part. Syst. Charact.* **2014**, *31*, 77–80.
40. Langille, M. R.; Personick, M. L.; Zhang, J.; Mirkin, C. A. Defining Rules for the Shape Evolution of Gold Nanoparticles. *J. Am. Chem. Soc.* **2012**, *134*, 14542–14554.
41. Lohse, S. E.; Burrows, N. D.; Scarabelli, L.; Liz-Marzán, L. M.; Murphy, C. J. Anisotropic Noble Metal Nanocrystal Growth: The Role of Halides. *Chem. Mater.* **2014**, *26*, 34–43.
42. Cañamares, M. V.; Chenal, C.; Birke, R. L.; Lombardi, J. R. DFT, SERS, and Single-Molecule SERS of Crystal Violet. *J. Phys. Chem. C* **2008**, *112*, 20295–20300.
43. Reigues, A.; Auguieb, B.; Etchegoin, P. G.; Le Ru, E. C. CW Measurements of Resonance Raman Profiles, Line-Widths, and Cross-Sections of Fluorescent Dyes: Application to Nile Blue A in Water and Ethanol. *J. Raman Spectrosc.* **2013**, *44*, 573–581.
44. Kumar, P. S.; Pastoriza-Santos, I.; Rodríguez-González, B.; García de Abajo, F. J.; Liz-Marzán, L. M. High Yield Synthesis and Optical Response of Gold Nanostars. *Nanotechnology* **2008**, *19*, 015606 (1–6).
45. Kelly, K. L.; Coronado, E.; Zhao, L. L.; Schatz, G. C. The Optical Properties of Metal Nanoparticles: The Influence of Size, Shape, and Dielectric Environment. *J. Phys. Chem. B* **2003**, *107*, 668–677.
46. Enustun, B. V.; Turkevich, J. Coagulation of Colloidal Gold. *J. Am. Chem. Soc.* **1963**, *85*, 3317–3328.
47. Scarabelli, L.; Grzelczak, M.; Liz-Marzán, L. M. Tuning Gold Nanorod Synthesis through Prereduction with Salicylic Acid. *Chem. Mater.* **2013**, *25*, 4232–4238.
48. Pérez-Juste, J.; Liz-Marzán, L. M.; Carnie, S.; Chan, D. Y. C.; Mulvaney, P. Electric-Field-Directed Growth of Gold Nanorods in Aqueous Surfactant Solutions. *Adv. Funct. Mater.* **2004**, *14*, 571–579.
49. Rodríguez-Fernández, J.; Pérez-Juste, J.; Mulvaney, P.; Liz-Marzán, L. M. Spatially-Directed Oxidation of Gold Nanoparticles by Au(III)-CTAB Complexes. *J. Phys. Chem. B* **2005**, *109*, 14257–14261.
50. Mayer, M.; Scarabelli, L.; March, K.; Altantzis, T.; Tebbe, M.; Kociak, M.; Bals, S.; García de Abajo, F. J.; Fery, A.; Liz-Marzán, L. M. Controlled Living Nanowire Growth: Precise Control over the Morphology and Optical Properties of AgAuAg Bimetallic Nanowires. *Nano Lett.* **2015**, *15*, 5427–5437.